Analyst

Accepted Manuscript

This article can be cited before page numbers have been issued, to do this please use: S. Arshavsky-Graham, K. Urmann, R. Salama, N. Massad-Ivanir, J. G. Walter, T. Scheper and E. Segal, *Analyst*, 2020, DOI: 10.1039/D0AN00178C.

View Article Online
DOI: 10.1039/D0AN00178C

ARTICLE

APTAMERS vs. ANTIBODIES AS CAPTURE PROBES IN OPTICAL POROUS SILICON BIOSENSORS

Sofia Arshavsky-Graham, [a,b,‡] Katharina Urmann, [a,b,‡] Rachel Salama, [b] Naama Massad-Ivanir, [b] Johanna-Gabriela Walter, [a] Thomas Scheper [a,*] and Ester Segal [b,*]

Received 00th January 20xx,
Accepted 00th January 20xx

DOI: 10.1039/x0xx00000x

Over the past decade aptamers have emerged as a promising class of bioreceptors for biosensing applications with significant advantages over conventional antibodies. However, experimental studies comparing aptasensors and immunosensors, under equivalent conditions, are limited and the results are inconclusive, in terms of benefits and limitations of each bioreceptor type. In the present work, the performance of aptamer and antibody bioreceptors for the detection of a his-tagged protein, used as a model target, is compared. The bioreceptors are immobilized onto a nanostructured porous silicon (PSi) thin film, used as the optical transducer, and the target protein is detected in a real-time and label-free format by reflective interferometric Fourier transform spectroscopy. For the antibodies, random-oriented immobilization onto the PSi nanostructure results in a poor biosensing performance. Contrary, Fc-oriented immobilization of the antibodies shows a similar biosensing performance to that exhibited by the aptamer-based biosensor, in terms of binding rate, dynamic detection range, limit of detection and selectivity. The aptasensor outperforms in terms of its reusability and storability, while the immunosensor could not be regenerated for subsequent experiments.

Introduction

Over the past 20 years, numerous publications and review articles have elaborated on the advantageous properties of aptamers as capture probes for biosensing [1-7]. Aptamers have been termed “chemical antibodies” and predicted to replace antibodies in the near future [3, 4, 8]. The possibility of selecting high affinity aptamers via SELEX (Systematic Evolution of Ligands by Exponential Enrichment) for a wide range of targets (including small molecules, proteins and whole cells), their small size, their high stability and outstanding performance in complex media have provoked the extensive research effort in their integration into various biosensing schemes [3, 9-11]. However, antibodies, which have been used as capture probes for biosensor design for over 70 years, are still considered as the “gold standard” [12, 13].

While some studies present results of different bioassays using antibodies or aptamers as capture probes towards the same target analyte [14-16], only few papers have experimentally compared between aptasensors and immunosensors under equivalent conditions [2, 5, 6, 17], and there is a lack of consensus in the field. Similar biosensing performance, in terms of selectivity and sensitivity, was demonstrated for quartz crystal-based biosensors for IgE detection [6] and nanogap impedance-based

[a] Institute of Technical Chemistry, Leibniz University of Hannover, Callinstr. 5, 30167 Hannover, Germany; Phone: +49-511-762-2509; email: scheper@iftc.uni-hannover.de
[b] Department of Biotechnology and Food Engineering, Technion Israel Institute of Technology, Technion City, 32000 Haifa, Israel; phone: +972-4-8295071; e-mail: esegal@technion.ac.il
‡ The authors contributed equally to this work.

† Footnotes relating to the title and/or authors should appear here.
Electronic Supplementary Information (ESI) available: [details of any supplementary information available should be included here]. See DOI: 10.1039/x0xx00000x

View Article Online
DOI: 10.1039/D0AN00178C

biosensor for thrombin detection [17]. However, the former also showed an extended linear detection range, reusability and greater stability for the aptasensor, in comparison to the immunosensor. In contrast, an aptasensor for detection of a prostate specific antigen showed a comparable limit of detection (LOD), selectivity, and reusability, to an immunosensor [2]. Both biosensors were based on nano-modified screen-printed electrodes, in three electrochemical detection techniques [2]. Recent reviews have also highlighted that antibody- and aptamer-based biosensors are comparable in their performance (i.e., sensitivity and selectivity), but emphasize that their immobilization onto the transducer and the detection mode have a more significant impact on the resulting sensitivity and selectivity [1, 16]. On the other hand, a superior biosensing performance of an aptamer over an antibody was observed in a porous silicon (PSi)-based optical biosensor for detection of insulin [5]. The aptamer outperformed the antibody in response value and time and LOD. However, it should be noted that in this study the antibody was covalently immobilized to the surface, resulting in a random orientation that limits its performance. This variability in the studies emphasizes the need for additional research in the field, specifically studying the behaviour of these capture probes on similar transducers and comparable conditions and characterizing the limitation and strength of each bioreceptor.

The present study aims to compare between aptamer and antibody capture probes, which are immobilized on the same nanostructured PSi-based transducer, for the detection of a specific target analyte and to investigate the performance and benefits of each receptor. PSi-based optical biosensors in which antibodies have been employed as capture probes were extensively studied over the past 20 years [18-22]. Many of these biosensors employ reflective interferometric Fourier transform spectroscopy (RIFTS) for real-time and label-free monitoring of changes in the refractive index or reflection intensity for various relevant targets, such as DNA [23], protein [5, 24, 25] and bacteria [26, 27]. The first application of aptamers as bioreceptors in PSi-based optical biosensors has been demonstrated in 2015 [28], showing promising biosensing results, which evoked a great interest. Since then, the potential of different PSi-based aptasensors has been increasingly studied and successful detection of various molecules was demonstrated [5, 24, 27, 29-33].

In our previous work [28, 31, 34, 35], we have successfully constructed and characterized several PSi aptasensors for various targets. In the present work, we focus on the direct comparison of the performance of PSi-based aptasensor and immunosensor for detection of the same target protein. To the best of our knowledge, this is the first comparison of aptamers to random- or oriented-immobilized antibodies as capture probes. An oxidized PSi ($PSiO_2$) nanostructure (Fabry-Pérot thin film), used as the optical transducer, was functionalized with a well-characterized his-tag binding aptamer (6H7) [31, 36-39] or an anti his-tag antibody for the detection of a model his-tagged protein, 6x-his tyrosinase from *Bacillus megatherium* (35.3 kDa). Successful conjugation of the capture probes onto the nanostructured $PSiO_2$ was confirmed by attenuated total reflectance Fourier transform infrared (FTIR-ATR) spectroscopy, and surface density was quantified by cleavage of the bioreceptors from the surface and subsequent fluorescence analysis. The binding of protein target molecules to the immobilized bioreceptors was monitored in real time by RIFTS and the biosensing performance, in terms of binding rate, dynamic range and sensitivity, was compared for the aptamer and the antibody-conjugated biosensors. The latter was further studied in a random or Fc-oriented conjugation to the $PSiO_2$ surface. Focus was laid especially on comparing the selectivity and the performance of both bioreceptors in the detection of the target protein within complex biological samples, utilizing bacteria lysates as a model, as well as the recyclability of the biosensors.

Experimental

Materials

Si wafers (p-type, boron doped, 0.00095 Ω·cm resistivity, <100>-oriented) were purchased from Siltronix Corp (France). Aqueous HF (48%) and ethanol absolute were purchased from Merck (Germany). Dimethyl sulfoxide (DMSO) and Toluene were purchased from Carlo Erba Reagents and Bio-Lab ltd, respectively. (3-aminopropyl)triethoxysilane (APTES), ethyldiisopropylamine (EDIPA), glutaraldehyde 25% solution (GA), ethanolamine, *N*-(3-Dimethylaminopropyl)-*N*-ethylcarbodiimide hydrochloride (EDC), succinic acid, sodium cyanoborohydride, sodium dodecyl sulfate (SDS), N-Succinimidyl 3-(2-pyridyldithio)propionate (SPDP), DL-Dithiothreitol (DTT), isopropyl alcohol (IPA) and buffer salts were supplied by MERCK (Israel). Buffers were prepared with deionized water (18.2 MΩ cm) and filtered prior to use. Anti-his-tag aptamer 6H7 (5'- GCT ATG GGT GGT CTG GTT GGG ATT GGC CCC GGG AGC TGG C - 3') sequence was taken from U.S. patent 7329742 [37] . 6H7 was selected in 50 mM K_2HPO_4, 150 mM NaCl, 0.05% Tween 20 (this buffer is subsequently abbreviated as SB-T). To prevent possible blocking of the amino-modified surfaces, Tween 20 was omitted during immobilization and washing steps, as well as renaturation of the aptamer (and this composition is termed as the selection buffer, SB). Additional buffers were phosphate buffered saline (PBS, 1 mM phosphate buffer, 154 mM $NaCl_2$, pH 7.4) and 4-(2-hydroxyethyl)-1-piperazineethanesulfonic acid) (HEPES), which were prepared according to standard recipes. Aptamers were purchased with a 5'-amino modification or a 5' thiol modification and 3' 6-FAM modification from Integrated DNA Technologies (USA). Mouse anti-his monoclonal antibody (catalogue number MCA1396) was obtained from Enco (Israel). This antibody was validated by the manufacturer for ELISA, immunoprecipitation and western blotting applications. Mouse anti-his monoclonal antibodies are commonly used for these applications, as well as for biological detection and purification assays [40-45]. Streptavidin and biotinylated protein A were purchased from Sigma-Aldrich Chemicals. Proteins for biosensing experiments included trypsin from porcine pancreas (Sigma-Aldrich Chemicals) and 6xhis tyrosinase from *Bacillus megatherium* (recombinant, expressed in *Escherichia coli*), generously supplied by Prof. Ayelet

View Article Online
DOI: 10.1039/D0AN01780

Fishman, Technion. As an additional negative control and for simulation of complex media, *Escherichia coli* (*E. coli*) lysates were used. For this purpose, *E. coli* strain JL-102 was cultured in Luria broth (LB) medium (10 g L^{-1} casein peptone, 10 g L^{-1} NaCl, 5 g L^{-1} yeast extract, all purchased from Sigma-Aldrich Chemicals).

Preparation of Bacteria Suspensions and Bacteria Lysates

A flask with 20 mL sterile LB medium was inoculated with 100 µL of a freeze culture of *E. coli* JL-102 (free of plasmids) and cultured overnight under shaking at 37°C. The resulting culture was used for biosensing experiments to mimic a biologically relevant complex fluid.

A volume of 2 mL of the bacteria culture was spun down in a standard lab centrifuge and the supernatant was replaced by 1 mL PBS selection buffer. Following the re-suspension, the culture was ultrasonicated at 4°C (Labsonic M, Sartorius Stedim Biotech, Germany). The resulting suspension was centrifuged again to remove cell debris and the supernatant was transferred to a fresh tube and further used as the bacteria lysate.

Preparation of Oxidized PSi ($PSiO_2$).

Silicon was anodized at a constant current density of 375 mA cm^{-2} for 30 s in a 3:1 (v/v) solution of aqueous HF (48%) and ethanol. The anodization setup is similar to previous work [28]. Briefly, a Si wafer with exposed area of 1.33 cm^2 was contacted on its back side with a strip of aluminium foil and mounted in a Teflon etching cell and a Platinum wire was used as the counter electrode. The freshly-etched PSi film was rinsed with ethanol several times and subsequently dried under nitrogen gas flow. The resulting PSi sample was then thermally oxidized at 800°C for 1 h in ambient air in a tube furnace (Thermo Scientific, Lindberg/Blue M™ 1200°C Split-Hinge, USA).

Characterization of $PSiO_2$ Films

Specific properties (i.e. thickness and porosity) of the fabricated $PSiO_2$ layers were characterized by several techniques: HRSEM (high resolution scanning electron microscopy), and SLIM (spectroscopic liquid infiltration method) methods, as previously described [18].

Immobilization of Aptamers onto $PSiO_2$

The anti-his-tag aptamer (6H7) was conjugated onto the surface of the $PSiO_2$ film by EDC-mediated covalent attachment [28]. $PSiO_2$ sample was first incubated with a 2% (v/v) APTES solution in toluene for 1 h. After thorough rinsing with toluene, ethanol, and acetone and drying under a nitrogen stream, the amine-modified surface was immersed in a freshly prepared solution of 100 mg of succinic acid in 4.7 mL of DMSO and 300 µL of 0.1 M $NaHCO_3$ (pH 9.4) for 30 min. After rinsing with DMSO and purified water and drying under a nitrogen stream, EDC solution at a concentration of 52 mM (in SB) was introduced and allowed to react for 1 h. Successively, the activated $PSiO_2$ surface was incubated with the aptamer solution (75 µM, 50 µL in SB) for 1 h, followed by thorough washing with 50 mM Tris buffer (pH 7.4) for 20 min, to block remaining active sites. Finally, the biosensor was exposed to boiling deionized water for 2 min and gently dried under a nitrogen stream to unfold any aptamer secondary structures. The resulting aptasensors were stored dried in a desiccator for up to 4 days post immobilization. Prior to biosensing experiments, the aptasensors were incubated in a solution of 1 M imidazole in SB (pH 7.4), followed by incubation in SB for 30 min, in order to allow the immobilized aptamer to properly fold.

Immobilization of Antibodies onto $PSiO_2$

The anti-his antibody was either directly immobilized via covalent binding, leading to a random antibody orientation, or conjugated via the biotin-streptavidin linkage to result in an oriented antibody configuration [26, 46].

For random antibody immobilization, the $PSiO_2$ surface was incubated with a solution of 1% APTES and 1% EDIPA in water for 30 min. After removing the solution, the sample was rinsed with water and ethanol, then dried under a nitrogen stream. Subsequently, the film was incubated in a 2% aqueous GA solution for 30 min, washed with water and dried under a stream of nitrogen. In the next step, 50 µL of the antibody solution (100 µg mL^{-1} in PBS) were introduced and incubated for 1 h at room temperature and then stored overnight at 8°C. Next, unbound antibodies were removed by thorough washing with PBS and residual reactive groups were capped by incubation of the porous film with 0.1 M aqueous solution of ethanolamine for 30 min.

For oriented antibody immobilization, silanization and modification with GA were performed as described above, followed by incubation with 50 mM sodium cyanoborohydride in HEPES for 30 min, in order to stabilize the Schiff base formed during reaction of the aldehyde groups with the amine groups [47]. After washing with HEPES, the $PSiO_2$ film was placed in a humidity chamber and 100 µL of a freshly-prepared streptavidin solution (100 µg mL^{-1} in PBS) were introduced onto the surface and incubated for 1 h. A thorough rinsing with PBS was performed before a repetition of the reduction in sodium cyanoborohydride for the stabilization of the Schiff base, formed during streptavidin fixation. Next, the streptavidin-modified surface was blocked with ethanolamine, followed by incubation with biotinylated protein A (100 µL; 100 µg mL^{-1} in PBS) for 1 h in a humidity chamber. Finally, the sample was rinsed with PBS and incubated with the antibody (50 µL; 100 µg mL^{-1} in PBS; humidity chamber) for 1 h at room temperature and then overnight at 8°C. On the next day, the film was rinsed and stored in PBS buffer (at 8°C) for up to one day prior to biosensing experiments.

Infrared Spectroscopy

Chemical modification steps were verified using attenuated total reflectance Fourier transform infrared (ATR-FTIR) spectroscopy. Spectra were recorded using a Thermo Fisher 6700 FTIR instrument equipped with a Smart iTR diamond ATR device (USA). Background and all sample spectra were measured in dry air, utilizing an IR source and a DTGS kBr

View Article Online DOI: 10.1039/D0AN01796D

detector. Number of scans was set to 256, at a resolution of 4. The samples were dried under a nitrogen stream before each measurement.

Bioreceptors Surface Density

For the antibody quantification, a FITC-labelled IgG was immobilized in a random or oriented-configurations within the $PSiO_2$ film, as described above. As a control, $PSiO_2$ films were chemically activated by the full chemistry procedure, but without antibody application. After immobilization, the samples were extensively washed with PBS and sodium acetate buffer (0.1 M, pH 4.5) to remove any unbound IgG molecules from the surface. The latter was confirmed by monitoring the fluorescence signal (excitation and emission wavelength values of 490 nm and 525 nm, respectively using a Thermo Scientific Varioskan Flash) of the washing solutions until no signal was measured, in comparison to the controls. Then, 250 µL of pepsin solution (100 µg mL^{-1} pepsin in sodium acetate buffer) was introduced onto the immunosensor and incubated for 24 h at 37 °C for proteolytic digestion. After 24 h, the solution was collected and replaced by a fresh pepsin solution for additional cleavage. The concentration of the IgG in the collected solution was determined by fluorescence measurements at excitation and emission wavelength values of 490 nm and 525 nm, respectively (Thermo Scientific Varioskan Flash). The measured fluorescence values were correlated to the respective IgG concentrations using a calibration curve, which was constructed using known concentrations of FITC-labelled IgG. For the calibration curve preparation, FITC-labelled-IgG was diluted in sodium acetate buffer, containing also biotinylated protein A and streptavidin, in the relevant concentrations applied for the immobilization chemistry procedure. Then, pepsin was added to a final concentration of 100 µg mL^{-1}, and the calibration curve samples were incubated for 24 h at 37 °C, followed by fluorescence analysis.

For the aptamer, we adapted the method described by Hu *et al* [48]. Following silanization with APTES (as described above), the amine-terminated surfaces were reacted with 6.5 mM N-Succinimidyl 3-(2-pyridyldithio)propionate (SPDP) in ethanol for 30 min and washed thoroughly with IPA and ddH_2O. Subsequently, 75 µM thiol modified and FAM6-labeled aptamer in HEPES buffer (0.05M HEPES, pH 7.5) was introduced and incubated for 1 h. The functionalized $PSiO_2$ was extensively rinsed with HEPES, to remove physisorbed aptamer molecules, until no fluorescence signal was observed for the collected washing solution (compared to a control, i.e., $PSiO_2$ which was similarly functionalized with SPDP, but without aptamer). It should be noted that the aptamer stock was diluted in TE buffer (10 mM Tris and 1 mM EDTA, pH 8.0) with 30 mM DTT and prior to its use, the aptamer was cleaned in NAP-5 column (GE healthcare) to remove the DTT reducing agent and replace the buffer with HEPES. The resulting aptamer-functionalized $PSiO_2$ was incubated with DTT solution (250 µL of 25 mM DTT in HEPES buffer, pH 7.5) for 24 h. The solution was collected and replaced by a new reducing solution and the fluorescence signal of the collected solution was measured using a plate reader at excitation and emission wavelength values of 490 nm and 525 nm, respectively. The cleavage process was repeated until no fluorescence signal was observed for the collected solution (compared to the control). The measured fluorescence values were correlated to the respective aptamer concentrations using a calibration curve, which was constructed using known concentrations of FAM6-labeled aptamer. For the calibration curve preparation, FAM6-labeled aptamer was dissolved in 25 mM DTT in HEPES buffer and the fluorescence of these solutions was measured.

The respective bioreceptor surface density values were calculated by dividing the number of bioreceptor moles by the porous surface area. The latter was measured in a previous study [49] by nitrogen adsorption isotherms and application of BET (Brunauer-Emmett-Teller) model for a similar $PSiO_2$ nanostructure, see Supporting Information.

Measurement of Interferometric Reflectance Spectra

Interferometric reflectance spectra of the samples were collected as was previously described [28]. Briefly, interferometric reflectance spectra of the $PSiO_2$ films were collected using an Ocean Optics charge-coupled device (CCD) USB 4000 spectrometer coupled with a microscope objective lens by a bifurcated fiber-optic cable (USA). A tungsten light source was focused onto the surface of the sample with a spot size of approximately 1–2 mm^2. The reflectivity spectrum of the $PSiO_2$ film is comprised of a series of Fabry–Pérot interference fringes, where the maxima of these fringes are governed by the following equation:

$$m \cdot \lambda = 2 \cdot n \cdot L \quad \text{Equation 1}$$

where, m is an integer, λ is the light wavelength, n is the average refractive index of the porous film and L refers to its thickness. The term 2nL represents the effective optical thickness (EOT), where a change in the latter indicates a change in the refractive index.

Reflectivity data were recorded every 30 s in a wavelength range of 400–1000 nm and spectral acquisition time 100 ms. The spectra were analysed by applying fast Fourier transformation (FFT), which leads to a single peak for each spectrum, whose position (corresponds to the value of 2*nL*, i.e., the EOT) was monitored. In this work, data are presented as relative ΔEOT, defined as:

$$\frac{\Delta EOT}{EOT_0} = \left(\frac{EOT_{readout} - EOT_{at\ baseline}}{EOT_{at\ baseline}}\right) \quad \text{Equation 2}$$

The term EOT_0 refers to the averaged EOT obtained during baseline measurement at the beginning of each optical experiment.

Protein Biosensing

Biosensing experiments were carried out in a cell configuration. The biofunctionalized $PSiO_2$ samples were mounted into a custom-made Plexiglas cell. An O-ring inside the cell seals off the exposed area and an in- and outlet allow introducing solutions for subsequent reaction steps. At first, spectra were

recorded until a stable baseline was achieved in either PBS or SB, depending on the respective capture probe. Functionalized $PSiO_2$ films were then incubated with 100 µL of the protein solution for 1 h (without flow). Tyrosinase was diluted in PBS or SB for the antibody or aptamer functionalized $PSiO_2$, respectively. The complex samples, including trypsin, lysate and spiked lysate, were prepared in SB-T for the aptamer-based biosensor to reduce nonspecific binding, according to previous studies [28]. After removal of the protein solution, the sample was rinsed and incubated for 30 min with PBS/SB. Each aptamer-based biosensor was utilized for multiple biosensing experiments, through surface regeneration, as previously described [28]. The protein was eluted with 1 M imidazole in SB (pH 7.4) for 30 min, followed by the regeneration of aptamers in SB for 30 min. Antibody-conjugated biosensors were used only once.

Regeneration of the oriented antibody biofunctionalized $PSiO_2$ was studied by exposure of the surface to different solutions for 30 min, as summarized in Table 1.

Table 1 Composition of regeneration solution for the oriented antibody-based biosensor

Solution Composition
1M imidazole in SB (pH 7.4)
10 mM glycine/HCl pH 2.5 [50]
100 mM glycine/HCl pH 2.5 [51]
100 mM HCl pH 2.0 [52, 53]
200 mM glycine/HCl pH 2.3 + 1% DMSO [54]
1% SDS in ddH_2O [55]

Statistical Analysis and Data Regression

For statistical analysis, unpaired t-tests were performed, with two tail distribution and unequal variance. Resulting two-tailed P values below 0.05 were required to consider the compared groups as significantly different from each other.

Non-linear regression of obtained data was performed with GraphPad Prism software utilizing the model for specific binding with hill slope. The following equation was used for modelling:

$$Y = \frac{B_{max} \cdot X^h}{(K_d^h \cdot X^h)} \qquad \text{Equation 3}$$

Herein, B_{max} is the interpolated concentration at which the maximum biosensor response is reached. K_D (also known as the apparent dissociation constant) is the target concentration needed to reach the half-maximum biosensing signal. The parameter h is the Hill coefficient, which gives information about the stoichiometry of the occurring binding [56, 57].

RESULTS AND DISCUSSION

Immobilization of Bioreceptor Molecules onto $PSiO_2$

The porous nanostructures were fabricated by anodization and subsequent thermal oxidation to yield $PSiO_2$ films with a thickness of 5500 nm and characteristic interconnected cylindrical pores with a typical diameter between 35 and 65 nm (see Table S1, Supporting Information, for a summary of the PSi nanostructure characteristics). Figure 1a (upper panel) schematically illustrates the immobilization of the amino-modified 6H7 aptamer onto the $PSiO_2$ film. The latter was first amino-silanized using APTES dissolved in toluene (2%) and subsequent carbodiimide coupling was employed to conjugate the amine-terminated 6H7 aptamers, as we previously reported [28, 31]. Successful aptamer conjugation was confirmed by ATR-FTIR spectroscopy. The spectra following each of the modification steps are presented in Figure 1b (upper panel). After the amino-silanization, a small peak at 1639 cm^{-1} is observed, attributed to the bending of the primary amines [58, 59]. Following the carboxylation of the surface with succinic acid, the spectrum depicts two strong peaks at 1556 and 1632 cm^{-1} attributed to amide II and amide I bonds, respectively, and a peak at 1400 cm^{-1} is assigned to the carboxylic acid groups [58, 59]. After EDC introduction, the carboxylic acid peak is observed to diminish, suggesting successful activation. Following aptamer conjugation, multiple characteristic DNA bands appear between 1780-1530 cm^{-1} and 1550-1250 cm^{-1}, attributed to the carbonyl groups and vibrations of saccharides [60], similarly to our previous report [28].

For the antibody immobilization, two different strategies were used (as schematically illustrated in Figure 1a, middle and bottom panels): (1) straightforward conjugation in random orientation via an amine-group within the antibody to an aldehyde-modified surface (this immobilization route will be referred as 'random conjugation'), and (2) oriented conjugation of the antibody Fc-region to a protein A-modified surface. For both immobilization routes, the $PSiO_2$ was first silanized using an aqueous APTES solution (1%). It should be noted that this step was slightly modified in comparison to the aptamer immobilization route to allow an optimal immunosensor performance (see Figure S1, Supporting Information). Next, the amine-activated $PSiO_2$ was reacted with glutaraldehyde. For the random immobilization route, the aldehyde-activated $PSiO_2$ surface was immediately incubated with the antibody solution. Thus, the antibody is conjugated through its primary amines to available aldehyde groups on the $PSiO_2$ surface. Following a thorough rinsing, residual amines were blocked by incubation with ethanolamine. For the oriented antibody conjugation, protein A layer was formed on a glutaraldehyde-reacted $PSiO_2$ surface through streptavidin-biotin linkage, followed by antibody conjugation to the protein A through the Fc-region, as shown in Figure 1a (bottom panel). For both conjugation routes, the conditions were optimized in previous studies [20, 26] to minimize steric hindrance and crowding effects.

Figure 1b, middle and bottom panels, present the ATR-FTIR spectra of the corresponding chemical modification steps for the random and oriented conjugation routes, respectively. For both, following amino-silanization, a peak at 1637 cm^{-1} appears, attributed to the bending of primary amines. Upon glutaraldehyde functionalization, peaks are observed at 1720, 1637, 1560, 1445 and 1401 cm^{-1}, which are ascribed to the (C=O) stretching vibrations, the imine bond, and (C-H) and (C-C) bond vibrations, respectively [60]. For the random conjugation route, antibody immobilization results in peaks at 1643 and 1555 cm^{-1}, which are attributed to the bending of amide I and amide II, respectively [58]. For the oriented conjugation route,

View Article Online
DOI: 10.1039/D0AN00178C

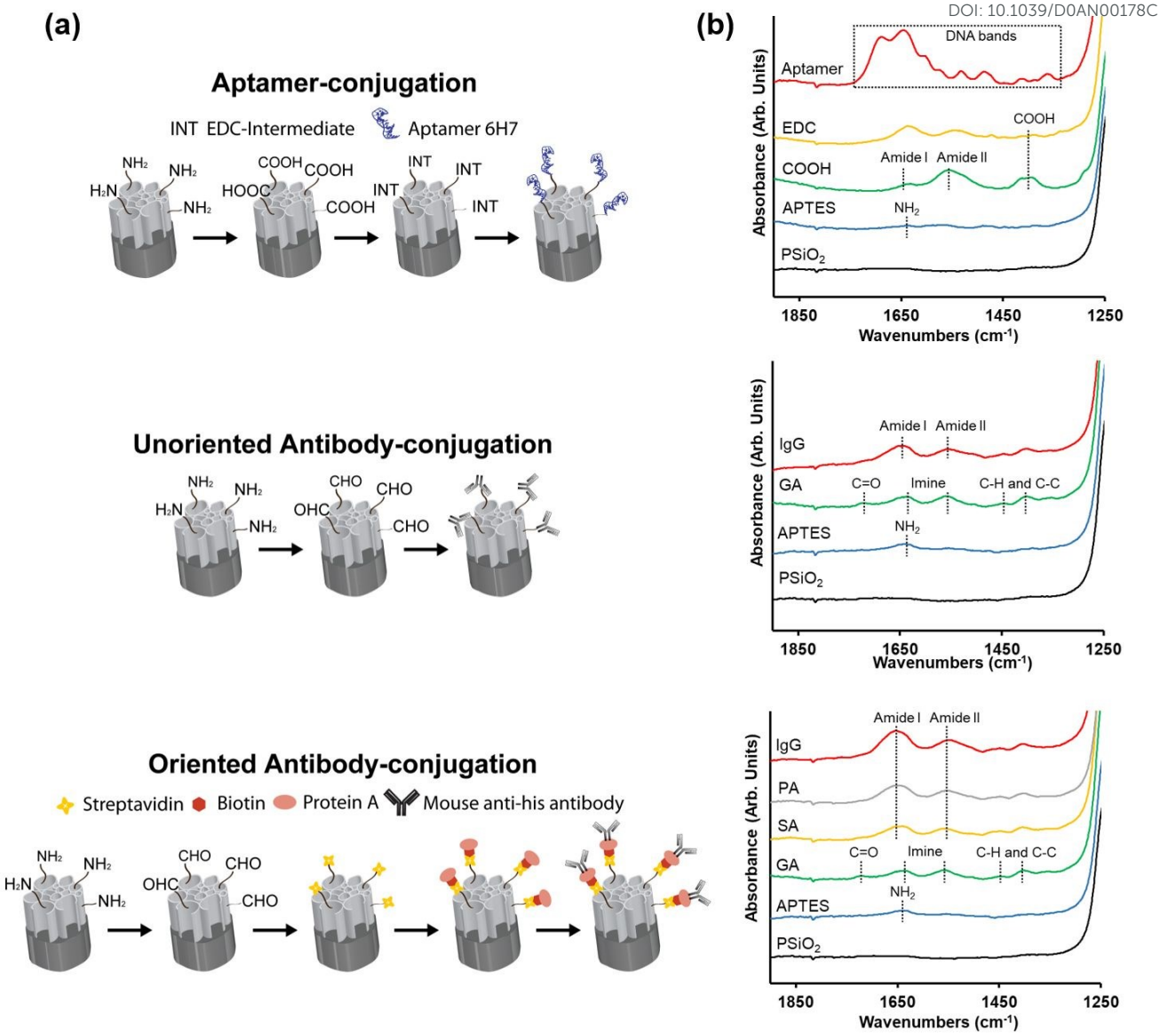

Fig. 1 (a) Schematic illustration of the coupling steps followed for the immobilization of aptamers (upper panel) and antibodies (via random and oriented conjugation, middle and bottom panels, respectively) to $PSiO_2$. (b) ATR-FTIR spectra of $PSiO_2$ upon the different chemical modification steps throughout aptamer and antibody immobilization on the surface.

similar peaks are observed for streptavidin, protein A and antibody immobilization, with greater absorbance respective to the preceding step, suggesting successful modification of the $PSiO_2$ film.

It should be emphasized that while chemical route for the construction of the immunosensor is well established, it involves multiple steps and the thus the immobilization procedure is >3 times longer (~4 times for the oriented antibody) in comparison to that of the aptasensor. Moreover, there are significant differences in the cost of the biosensors, which results from both the price of the bioreceptors and the reagents used for their immobilization. Thus, the immunosensors cost is >5 times higher than that of the aptasensors.

Bioreceptors Surface Density

Surface density has a major impact on the performance of biosensors. It determines the bioreceptor orientation, the uniformity of the sensing layer and the steric crowding within the sensing layer [61, 62]. It also influences the target capture kinetics and the overall sensitivity of the biosensor [63, 64]. Thus, the bioreceptor surface coverage for the aptasensor and the immunosensor was determined by quantifying the amount of immobilized aptamer and antibody, respectively, onto the $PSiO_2$ surface. In both cases, the immobilized bioreceptors were cleaved from the respective biosensor and their concentration in the solution was measured, as illustrated in Figure 2. For the immunosensor, a fluorescently labelled antibody (in which the fluorophore is conjugated to the amine groups) was immobilized in a random or oriented configuration; after which,

View Article Online
DOI: 10.1039/D0AN00178C

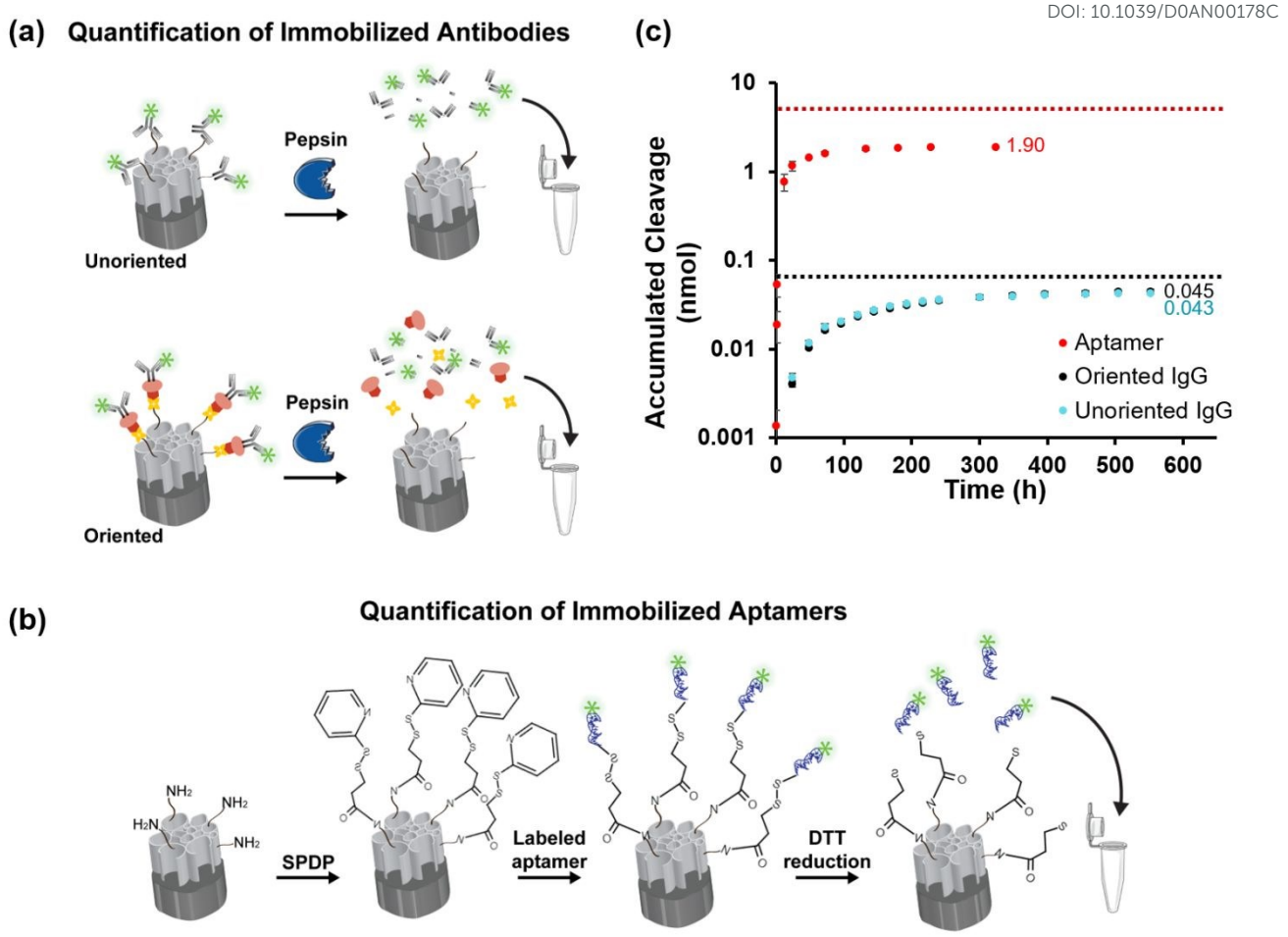

Fig. 2 Bioreceptors surface density. Schematic illustration of the quantification method used for (a) the immunosensors and (b) the aptasensors. (c) The accumulated number of moles of aptamer and antibody molecules (oriented and unoriented) cleaved from the $PSiO_2$ surface vs. time (n = 3). The dashed lines represent the applied amount of the respective bioreceptor during immobilization.

the functionalized surface was subjected to proteolytic digestion (using pepsin), as depicted in Figure 2a. The pepsin cleaves the IgG into ($F(ab')_2$) molecules, and the Fc fragment (as well as other proteins) into lower molecular weight fragments [65]. Thus, following digestion, these cleaved fragments are released to the solution and quantified (by fluorescence measurements). For the immobilized aptamer, a fluorescently-labelled and thiol-modified aptamer was conjugated to the surface using SPDP linker, as illustrated in Figure 2b. This allows to cleave the immobilized fluorescent aptamer by disulphide bond reduction and subsequent quantification of the solution fluorescence, as described by Hu *et al* [48].

Figure 2c presents the accumulated moles of antibody and aptamer cleaved from the surface vs. time. For the aptamer, the cleavage is fast and the accumulated amount of the "released" aptamer stabilizes within 24 h. For the antibody, the cleavage is much slower, as the relatively large pepsin molecules are required to infiltrate into the porous layer to catalyse the digestion, followed by out diffusion of the resulting protein fragments to the solution. For the aptamer, a total amount of 1.89±0.02 nmol was released, which is approximately half of the aptamer amount used for the conjugation. For the oriented and unoriented antibody, the total amount was 0.045±0.002 and 0.0430±0.0006 nmol, respectively, which is two orders of magnitude lower than that of the aptamer. As the specific surface area for both biosensors are similar, the significant difference in the amount of the immobilized bioreceptors correlate to the respective calculated surface density (see Table S2, Supporting Information). Thus, the results demonstrate the significantly higher surface density of the aptamer molecules immobilized within the porous nanostructure film, compared to the antibodies. This is mainly ascribed to the profound differences in the size of the two bioreceptors; where the aptamer is approximately >10-fold smaller than the antibody [3, 6, 66], which enables higher immobilization density and surface coverage. Thus, for the aptasensor, a greater number of binding sites are available for the target within the same nanostructure, compared to the immunosensor [6, 67]. This in turn is highly advantageous for enhancing the sensitivity of the biosensor [63].

It should be emphasized that although a different immobilization chemistry was utilized for quantifying the aptamer surface density (and as such the total number of

View Article Online
DOI: 10.1039/D0AN00178C

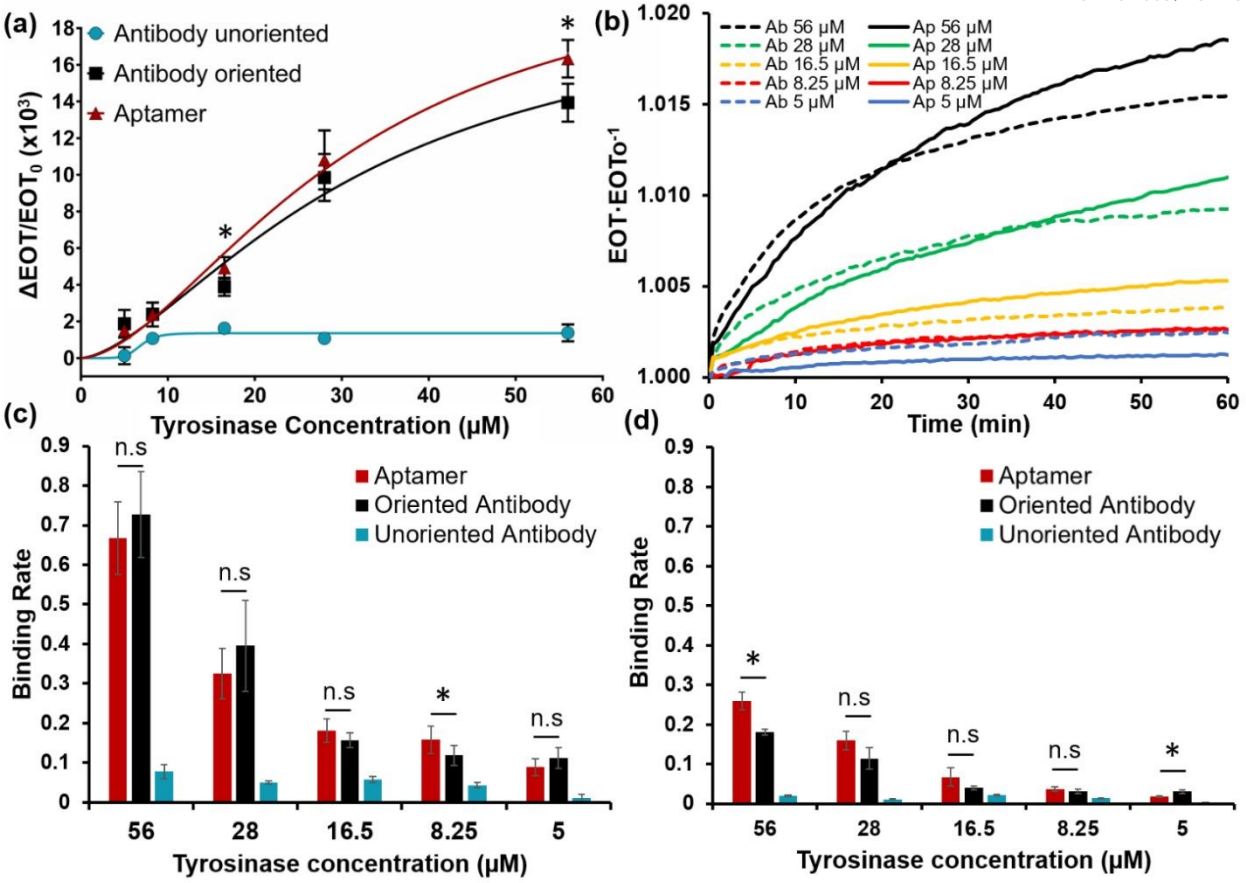

Fig. 3 (a) Relative EOT changes of different $PSiO_2$ biosensors (random and oriented antibody-conjugated $PSiO_2$ and aptamer-conjugated $PSiO_2$) collected after 1 h exposure to varying tyrosinase concentrations. The lines show the curves fitted for specific binding with Hill slope. (b) Relative EOT changes vs. time for oriented antibody (Ab)- or aptamer (Ap)-immobilized $PSiO_2$ upon exposure to different concentrations of his-tagged tyrosinase (data represents an average of n ≥ 3). (c) and (d) Binding rates [$(EOT \cdot EOT0^{-1} \cdot min^{-1}) \cdot 10^3$] at 10 min and 60 min of incubation with different tyrosinase concentrations, respectively, for the three types of biosensors. (n.s) or (*) Indicate non-significant or statistically significant difference, respectively, between total binding or the binding rate of the oriented antibody and aptamer-based biosensors (t test, n ≥ 3, $p < 0.05$).

immobilized aptamer molecules is not accurate), its effect on the obtained value may be neglected due to the profound difference of 2-orders of magnitude in surface densities between the aptasensor and immunosensor. In addition, for the immunosensor constructed via random conjugation, our quantification method underestimates the total number of immobilized antibody molecules (see Table S1, Supporting Information). As in this case the antibodies are covalently bound to the porous surface, a fragment of the antibody is expected to remain attached to the surface after pepsin digestion, resulting in an incomplete cleavage. This is in contrast to the oriented immobilization, where the antibodies are conjugated to the protein A layer, which is digested by the pepsin, leading to a complete release of the immobilized antibodies.

Biosensing Experiments

For the biosensing experiments, the antibody-conjugated and the aptamer-conjugated $PSiO_2$ films were exposed to different protein solutions (5 μM to 56 μM) and Figure S2 (Supporting Information) presents characteristic results in terms of the relative EOT changes vs. time. Initially, PBS or SB (for antibody- and aptamer-conjugated $PSiO_2$, respectively) were introduced to establish a stable EOT baseline. Next, different analyte solutions were introduced onto the studied biosensor and allowed to react with the respective functionalized surface for 1 h (without flow). Subsequently, the biosensors were extensively rinsed with buffer (PBS or SB) to remove unbound molecules until a stable baseline is reached.

Figure 3a presents the averaged EOT values (attained after 1 h incubation with the target and subsequent washing with the buffer) for increasing protein concentrations and the corresponding curve fit utilizing a model for specific binding with Hill slope (see Equation 3). Oriented antibody and aptamer-based biosensors result in a target binding behaviour that can be modelled according to Equation 3, with a good fit (R^2=0.9490 and R^2=0.9731, respectively). For the unoriented immunosensor, no statistically significant differences were observed between the EOT signals measured for the different protein concentrations. Thus, owing to the poor performance of this biosensor, which is discussed in detail at the end of this section, we focus our discussion on the comparison between the aptasensor and oriented immunosensor. The dynamic range of these biosensors is from 8.25 μM to 56 μM, and the lowest measured target concentration is 5 μM, with an average

View Article Online
DOI: 10.1039/D0AN00179C

relative ΔEOT signal of 1.9±0.8 and 1.5±0.3 for the oriented-immunosensor and aptasensor, respectively. These signals can be reliably distinguished from the baseline, with a baseline noise equivalent to three standard deviations of 0.4 and 0.3 for the immunosensor and aptasensor, respectively. The observed micromolar detection limit agrees with the common limit of detection (LoD) values of label-free PSi-based optical biosensors [68]. We ascribe this high value mainly to mass transfer phenomena, specifically to the diffusion rate to and within the $PSiO_2$ nanostructure which has a profound effect at lower target concentrations [21, 63, 69-71]. This in fact does not allow a proper comparison between both bioreceptors in the lower detection range, as both biosensors are limited by the $PSiO_2$ transducer, regardless of the bioreceptor type. Thus, we cannot draw a conclusion on which of the bioreceptor results in improved biosensor sensitivity.

Overall, both biosensors perform in a similar manner, in terms of their dynamic range and sensitivity. This is also apparent in the binding rates for the aptamer and oriented antibody-based biosensors. Figure 3b depicts real time changes in the relative EOT signal (with respect to the baseline) for the oriented-antibody and aptamer-based biosensors upon incubation with increasing concentrations of tyrosinase. Both biosensors exhibit a similar target binding trend and a concentration-dependent behaviour. The calculated binding rates are presented in Figures 3c and 3d, as the initial (0 to 10 min) and total (0 to 60 min) values for different concentrations of tyrosinase, respectively. An insignificant difference is observed between both types of biosensors, regardless of the analysed duration, i.e. the initial or the total binding rate. The only apparent difference is observed at a longer binding time of 60 min, where the immunosensor reaches almost equilibration, while the signal for the aptasensor is far from surface saturation and keeps increasing (see Figure 3b). This behaviour is ascribed to the greater number of available binding sites for the target protein in the aptamer-based biosensor, in comparison to the antibody-based one (see Figure 2c). This also results in greater signal values for target concentrations ≥16.5 µM, as observed in Figure 3a. The greater number of available protein binding sites for the aptamer-based biosensor, maximizes target capture onto the $PSiO_2$ surface and consequently resulting in a higher signal [48].

The performance of the randomly conjugated antibody-immunosensor was generally poor. A significantly lower EOT signals were observed (see Figure 3a), as well as 10-fold lower binding rates, compared to the oriented antibody and aptamer-based biosensors (see Figure 3c and 3d). Also, a poor dependence of the binding rate in the protein concentration is found (see Figure S3, Supporting Information). Antibody conjugation via its primary amines is typically highly random, owing to the large number of amine groups in the antibody structure [72-76]. Thus, the functionality of these antibodies varies dramatically, and the resulting performance of the biosensors is limited. Since the total amount of antibodies immobilized within the porous layer for the random conjugation is similar or higher than for the oriented conjugation route, these results indicate that for the random conjugation less than ~10% of the immobilized antibodies are active, compared to the oriented immobilization. Our results suggest that immobilization of antibodies via a random amine-functionality is not preferable for fabrication of robust and specific $PSiO_2$ biosensors and this is in agreement with other biosensing systems [77-80]. The similar binding rate, dynamic detection range and sensitivity of the oriented antibody and aptamer-based biosensors indicate that by optimization of the bioreceptor immobilization, e.g., oriented vs. random antibody conjugation, a similar performance can be achieved utilizing the same transducer. Immobilization of the antibodies in an oriented configuration increases the active portion of the antibodies [76-78], resulting in a similar biosensing performance to that of the aptasensor, in which the aptamers are immobilized in a naturally orientated configuration at a much higher density.

Selectivity and Performance in Complex Samples.

$PSiO_2$ biosensors modified with 6H7-aptamer have previously demonstrated high selectivity towards their target his-tagged protein and robustness against unspecific adsorption even in complex media with an abundancy of non-target proteins (*i.e.* bacteria lysates) [28, 31]. In the present study, we compare the behaviour of the different biosensors upon exposure to non-target proteins (i.e., trypsin and bacteria lysate) and to complex media (bacteria lysate with a typical protein content of 1.8 mg mL^{-1}) spiked with the target tyrosinase. The optical response of the biosensors is summarized in Figure 4.

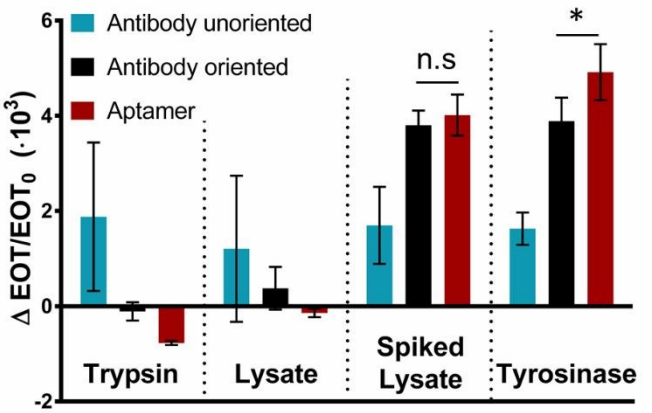

Fig. 4 The biosensor response, expressed as the relative EOT change, collected after 1 h exposure to different samples: trypsin as a non-target protein (concentration 16.5 µM), bacterial lysates (with a protein concentration of 1.8 mg mL^{-1}) and lysates spiked with 16.5 µM tyrosinase. The response of the biosensors to a pure tyrosinase (concentration 16.5 µM) solution is presented for comparison. (n.s) or (*) Indicate non-significant or statistically significant difference, respectively, between the oriented antibody and aptamer-based biosensors (t test, $n \geq 3$, $p < 0.05$).

Biosensors functionalized with aptamers and oriented antibodies show high affinity towards their target with reproducible results. The biosensors selectively detect their target protein in a complex solution of bacteria lysate and the obtained EOT values are in good agreement with the values collected for tyrosinase in a buffer (see also Figure 3 and Figure S4 for the real-time optical response). Notably, both biosensors exhibit low nonspecific adsorption of non-target proteins. We note that the negative response of the aptasensor to trypsin

View Article Online DOI: 10.1039/D0AN01786C

and lysate solutions may be ascribed to conformational changes of the immobilized aptamers. The latter are often utilized as the sensing mechanism in various aptasensors [81, 82].

Contrary, biosensors in which the antibody is conjugated in a random orientation exhibit similar response to all studied solutions and poor reproducibility, as can be seen by the large deviations obtained upon exposure to trypsin or bacteria lysates. Thus, the signals obtained for samples containing the pure target protein are indiscernible from those collected for non-target proteins. The inconsistent behaviour of antibody-regions other than the antigen binding sites is ascribed to the undirected immobilization, which may promote nonspecific adsorption onto the biosensor.

Biosensor Regeneration

One of the main advantages of DNA or RNA aptamers in comparison to antibodies is their ability to undergo reversible folding and unfolding, leading to a greater stability and a simpler elution of the bound target from the aptamer [83]. Thus, rendering aptamer-based biosensors as potentially recyclable [2, 6, 84]. For the 6H7 aptamers, exposure to imidazole enables the release of the bound target protein, by a competitive interaction between the imidazole, his-tagged target and the aptamer, similarly to the purification procedure of his-tagged proteins by immobilized metal ion affinity chromatography (IMAC) [28, 85]. Our previous report demonstrated the reusability of the 6H7 aptamer-functionalized $PSiO_2$ surface for up to 12 consecutive cycles by regenerating the biosensor surface in between these cycles by a short exposure to imidazole solution [28]. Contrary, the regeneration of immunosensors for repetitive usage is more complicated since antibodies are prone to irreversible denaturation [51]. While for aptamers regeneration conditions can be predefined during their selection in the SELEX process [86], for antibodies, regeneration must be investigated by a trial and error process for each antibody-antigen couple and biosensor platform [50, 51], owing to the different attractive forces defining each interaction and the stability of the transducer and signal to environmental changes [51]. Regeneration of immunosensors has been commonly achieved using acidic pH [52, 53], glycine/HCl [50, 52, 54], addition of detergents such as sodium dodecyl sulphate (SDS) [55] or addition of dimethyl sulfoxide (DMSO) [54]. Table 1 summarizes the different regeneration protocols which were employed for the oriented-antibody functionalized $PSiO_2$. All regeneration attempts were carried out at a high tyrosinase concentration (56 µM) which poses the greatest challenge for regeneration. The relative EOT changes upon exposure of the immunosensor to the different regeneration conditions, following a biosensing experiment of 56 µM target protein, are presented in Figure S5. None of these conditions was found to result in full restoration of the initial baseline; however, incubation in solutions of 1 M imidazole, 10 mM glycine/HCl pH 2.5 or 100 mM HCl (at pH 2.0) had the best effect. Next, we studied the reusability of the immunosensor in three consecutive cycles, where the biosensor was regenerated for 30 min in between the cycles utilizing these three regeneration solutions, see Figure S6. It should be noted that we performed a 30 min exposure of the immunosensor to the regeneration solution for a proper comparison to the aptasensor. Nevertheless, a shorter regeneration of 5 min results in a similar regeneration performance, see Figure S7, indicating that the exposure time (in this solution) has a negligible effect. Baseline drift in successive experiments, i.e., incomplete return to the original EOT value following exposure to the regeneration solution, was observed for all studied conditions, as shown in Figure S6. It should be pointed out that despite the harsh regeneration conditions (combination of low pH and relatively long exposure of 30 min to the regeneration solution), a maximal EOT decrease of only ~56% is achieved (for the use of 1M imidazole), indicating that the protein target was only partially eluted. Moreover, this moderate decrease in the EOT values also suggests that possible elution of the antibody molecules, due to possible disruption of the IgG binding to the immobilized protein A [87], is minor (the antibody molecular weight is ~5 times higher than that of the target protein and thus its elution should induce a pronounced decrease in the EOT value [69]). Based on the results presented in Figure S6, the combination of 10 mM glycine/HCl pH 2.5 (see Figure S6-III) was used for our subsequent studies as the achieved biosensing performance, in terms of the attained new signal in comparison to that achieved during the first biosensing cycle, was found to be better. For example, 80% compared to 55% for 10 mM glycine/HCl pH 2.5 and 1M imidazole, respectively, for the second biosensing cycle compared to the first.

Figure 5 summarizes the results of the biosensors' regeneration experiments. Figure 5b presents the attained EOT signals (expressed as percent of the first biosensing cycle signal) of the oriented-antibody and the aptamer-immobilized $PSiO_2$ upon three consecutive biosensing experiments. The biosensors were exposed to a high concentration of the target protein (56 µM) followed by a regeneration step (using 10 mM glycine/HCl pH 2.5 for the immunosensor and 1 M imidazole for the aptasensor). The characteristic real-time biosensing curves for these experiments are depicted in Figures 5c and 5d. Following the first regeneration step, the aptasensor performance has decreased by ~10%, see Figure 5b. Yet, after this initial decrease, the biosensor response was highly reproducible upon subsequent cycles, demonstrating a fair recyclability. It should be noted that a full baseline restoration after each biosensing cycle is not achieved (see Figure 5c). This is in contrast to our previous report for the 6H7 aptasensor [28] and may be attributed to the high target concentration used here, as well as to the different protein targets (tyrosinase vs. lipase). It is well established that the high structural complexity of proteins allows aptamer binding in different modes through a variety of attractive forces, which in turn significantly affects the binding strength [51, 66]. For the immunosensor, a greater activity loss of ~20% is observed in the second biosensing cycle, and by the third cycle, the collected signal is further decreased to 58±9%. Thus, regeneration of the immunosensor is not achieved using the common regeneration conditions studied here. This can be ascribed to the poor structural stability of the antibody following its denaturation, compared to the aptamers [6], and may require a further tedious probing of different regeneration

View Article Online
DOI: 10.1039/D0AN00178C

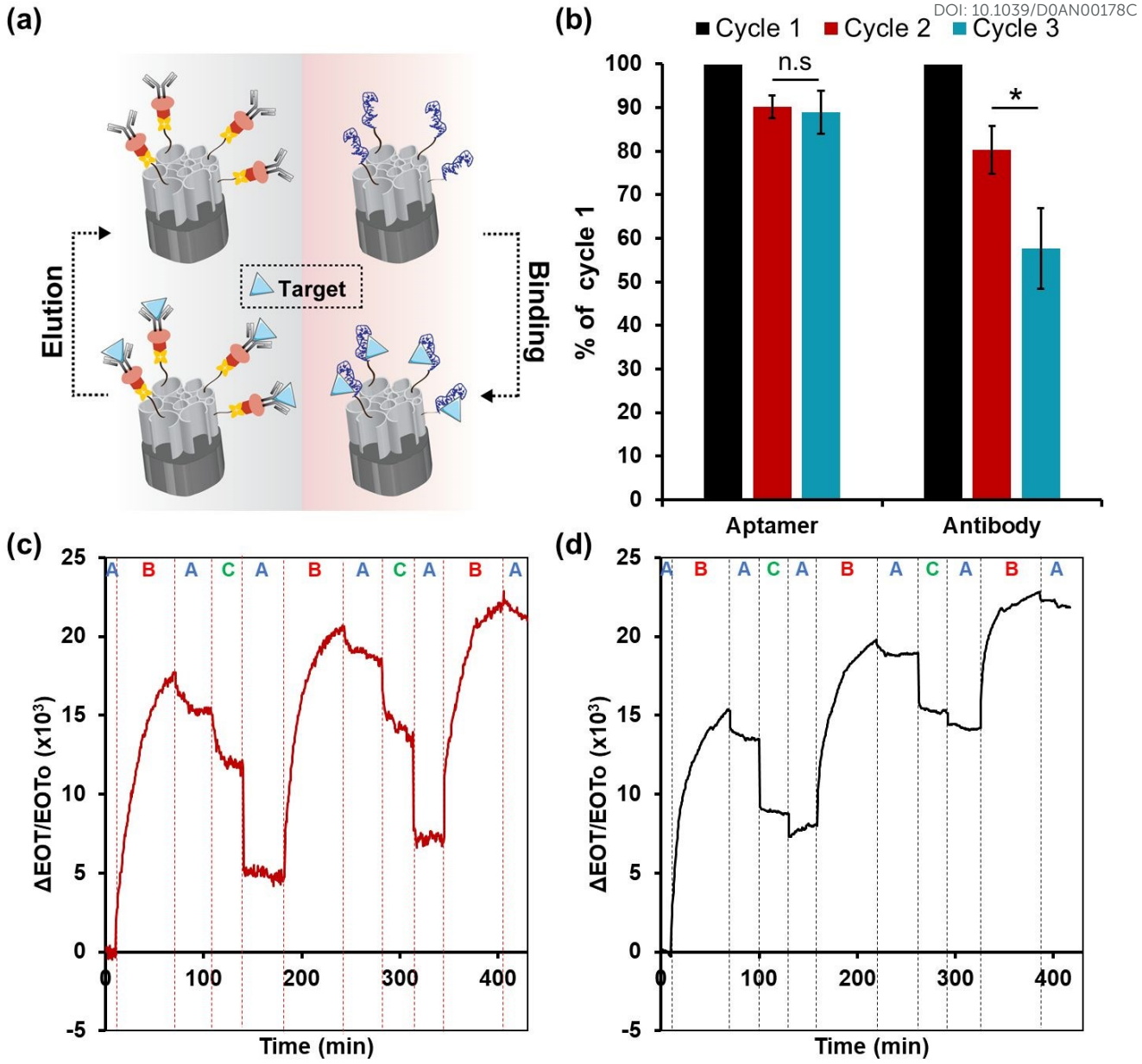

Fig. 5 (a) Schematic illustration of the biosensor regeneration concept. (b) Relative signal (presented as % of the EOT signal collected in the first biosensing cycle) collected from the (oriented) antibody- and the aptamer- biofunctionalized $PSiO^2$ upon three successive exposure cycles to 56 µM tyrosinase. After each exposure to the protein, the biosensors were regenerated with solutions of 10 mM glycine/HCl pH 2.5 or 1 M Imidazole supplemented SB, for antibody or aptamer biosensors, respectively. (n.s) or (*) indicate non-significant or statistically significant difference, respectively, between the oriented antibody and aptamer-based biosensors (t test, $n \geq 3$, $p < 0.05$). Relative EOT changes vs. time upon exposure of the (c) aptamer and (d) oriented antibody-biofunctionalized $PSiO_2$ to 56 µM Tyrosinase in three consecutive biosensing cycles, utilizing a regeneration solution of 1M imidazole for the aptasensor and 10 mM glycine/HCl pH 2.5 for the immunosensor. A, B and C indicate incubation with SB or PBS buffers, with the target protein or with elution buffer, respectively.

conditions for the immunosensor. The better performance of the aptasensor in the successive cycles can be also referred to the greater number of binding sites available for the target, due to the higher immobilization density of the aptamers. Thus, although full restoration of the biosensor is not achieved after each biosensing cycle, there are still sufficient binding sites for the target, at this high target concentration (56 µM). This makes the aptasensor reusable for at least three biosensing experiments of 56 µM tyrosinase, and could potentially be utilized for up to 12 consecutive biosensing cycles, according to our previous work [28]. It should be noted that in this work we have utilized imidazole as the eluting agent similarly to IMAC columns; however, aptamers can be also reversibly unfolded to release their target by a simple heat denaturation [86], which is not applicable for immunosensors. Thus, for potential practical application, the PSi-based aptasensors can be easily regenerated by heat treatment, which will further simplify the regeneration process.

Conclusions

This study presents a direct comparison for the specific detection of a model target protein, his-tagged tyrosinase, with antibody and aptamer capture probes, utilizing optical PSi-based biosensors. The 6H7 aptamer is compared to anti-his-tag antibodies, where the latter are immobilized onto the $PSiO_2$ nanostructure in a random or Fc-oriented configuration. The aptamer´s smaller size allows surface immobilization at much higher density, resulting in a larger number of binding sites on a similar $PSiO_2$ surface. However, in practice, both the aptamer and the oriented antibody-based biosensors present a similar biosensing performance in terms of the dynamic detection range, measured detection limit, binding rate and selectivity. Thus, the oriented conjugation route of the antibodies allows for similar performance even though the biosensor target binding capacity is smaller.

In contrast, a simple random immobilization of antibodies onto the $PSiO_2$ biosensors does not allow target detection. Although their surface density is comparable to that achieved by oriented immobilization, only ~10% of the randomly oriented antibodies were active. Thus, the laborious directed immobilization of the antibodies, even though decreasing the available free porous volume, and extending the fabrication time and costs, is required for successful target detection. Our main conclusion from the study is that by tailoring the immobilization chemistry and orientation of the bioreceptor, a similar biosensing performance can be achieved on the same transducer.

The aptasensor advantages are reflected in the practical fabrication, use and storage of the biosensor. The aptasensor fabrication is much faster and cost effective, compared to the immunosensor. Also, the high stability of the DNA aptamers allows for the aptasensor effective storage in dry conditions at room temperature before usage. Contrary, the immunosensor should be stored in a refrigerator in wet conditions, limiting its long-term storage. Importantly, the aptamer's ability to undergo reversible denaturation enables regeneration of the aptasensor for multiple uses. In contrast, the immunosensor cannot be regenerated without a significant activity loss after the first biosensing cycle.

It should be also pointed out that at lower target concentration, the sensitivity of both biosensors has been mainly limited by the PSi transducer, leading to a similar detection limit. Thus, the performance of both bioreceptors at the lower detection range could not be effectively compared. Our future work focuses on improving the limited sensitivity, while in the present work our main attention is directed to the comparison of the capture probes.

Conflicts of interest

There are no conflicts to declare.

Acknowledgements

This work was funded by the German Research Foundation under the grant SCHE 279/32-1. We thank Prof. Ayelet Fishman and her group at the Department for Biotechnology and Food Engineering at the Technion - Israel Institute of Technology, for supplying target proteins. ES, SAG, NM and KU acknowledge the core services and support from the Lorry I. Lokey Center for Life Science and Engineering. The authors also wish to thank the student Sharon Nissinmann for her help in some of the biosensing experiments. SAG is most grateful for the Russell Berrie Nanotechnology Excellence Scholarship for Graduate Students.

References

1. V. Crivianu-Gaita and M. Thompson, *Biosensors & bioelectronics*, 2016, **85**, 32-45.
2. M. Srivastava, N. R. Nirala, S. K. Srivastava and R. Prakash, *Scientific Reports*, 2018, **8**, 1923.
3. S. Song, L. Wang, J. Li, C. Fan and J. Zhao, *Trends in Analytical Chemistry*, 2008, **27**, 108-117.
4. D. H. J. Bunka and P. G. Stockley, *Nat. Rev. Microbiol.*, 2006, **4**, 588-596.
5. R. Chhasatia, M. J. Sweetman, F. J. Harding, M. Waibel, T. Kay, H. Thomas, T. Loudovaris and N. H. Voelcker, *Biosensors and Bioelectronics*, 2017, **91**, 515-522.
6. M. Liss, B. Petersen, H. Wolf and E. Prohaska, *Analytical Chemistry*, 2002, **74**, 4488-4495.
7. M. A. Morales and J. M. Halpern, *Bioconjug Chem*, 2018, **29**, 3231-3239.
8. T. Hianik and J. Wang, *Electroanalysis*, 2009, **21**, 1223-1235.
9. N. Duan, S. J. Wu, S. L. Dai, H. J. Gu, L. L. Hao, H. Ye and Z. P. Wang, *Analyst*, 2016, **141**, 3942-3961.
10. W. Zhou, P.-J. Jimmy Huang, J. Ding and J. Liu, *Analyst*, 2014, **139**, 2627-2640.
11. S. Ding, C. Mosher, X. Y. Lee, S. R. Das, A. A. Cargill, X. Tang, B. Chen, E. S. McLamore, C. Gomes, J. M. Hostetter and J. C. Claussen, *ACS Sensors*, 2017, **2**, 210-217.
12. M. Labib, E. H. Sargent and S. O. Kelley, *Chemical Reviews*, 2016, **116**, 9001-9090.
13. P. J. Conroy, S. Hearty, P. Leonard and R. J. O'Kennedy, *Seminars in cell & developmental biology*, 2009, **20**, 10-26.
14. X. Zhang, M. Sun, Y. Kang, H. Xie, X. Wang, H. Song, X. Li and W. Fang, *Toxicon*, 2015, **106**, 89-96.
15. H. Modh, T. Scheper and J. G. Walter, *Engineering in Life Sciences*, 2017, **17**, 923-930.
16. T. Hianik, *Electroanalysis*, 2016, **28**, 1764-1776.
17. U. Schlecht, A. Malavé, T. Gronewold, M. Tewes and M. Löhndorf, *Analytica Chimica Acta*, 2006, **573-574**, 65-68.
18. N. Massad-Ivanir, G. Shtenberg, T. Zeidman and E. Segal, *Advanced Functional Materials*, 2010, **20**, 2269-2277.
19. K. P. S. Dancil, D. P. Greiner and M. J. Sailor, *J. Am. Chem. Soc.*, 1999, **121**, 7925-7930.
20. L. M. Bonanno and L. A. DeLouise, *Langmuir*, 2007, **23**, 5817-5823.
21. M. P. Schwartz, S. D. Alvarez and M. J. Sailor, *Anal Chem*, 2007, **79**, 327-334.
22. T. Tieu, M. Alba, R. Elnathan, A. Cifuentes-Rius and N. H. Voelcker, *Advanced Therapeutics*, 2019, **2**, 1800095.
23. R. Vilensky, M. Bercovici and E. Segal, *Advanced Functional Materials*, 2015, **25**, 6725-6732.
24. S. Mariani, L. Pino, L. M. Strambini, L. Tedeschi and G. Barillaro, *ACS Sensors*, 2016, **1**, 1471-1479.
25. S. Mariani, V. Robbiano, L. M. Strambini, A. Debrassi, G.

Egri, L. Dähne and G. Barillaro, *Nature Communications*, 2018, **9**, 5256.
26. N. Massad-Ivanir, G. Shtenberg, N. Raz, C. Gazenbeek, D. Budding, M. P. Bos and E. Segal, *Scientific Reports*, 2016, **6**, 38099.
27. K. Urmann, S. Arshavsky-Graham, J. G. Walter, T. Scheper and E. Segal, *Analyst*, 2016, DOI: 10.1039/C6AN00810K.
28. K. Urmann, J.-G. Walter, T. Scheper and E. Segal, *Analytical Chemistry*, 2015, **87**, 1999-2006.
29. M. Terracciano, L. De Stefano, N. Borbone, J. Politi, G. Oliviero, F. Nici, M. Casalino, G. Piccialli, P. Dardano, M. Varra and I. Rea, *RSC Advances*, 2016, **6**, 86762-86769.
30. K. Urmann, P. Reich, J. G. Walter, D. Beckmann, E. Segal and T. Scheper, *J Biotechnol*, 2017, **257**, 171-177.
31. S. Arshavsky-Graham, N. Massad-Ivanir, F. Paratore, T. Scheper, M. Bercovici and E. Segal, *ACS Sensors*, 2017, **2**, 1767-1773.
32. M. Terracciano, I. Rea, N. Borbone, R. Moretta, G. Oliviero, G. Piccialli and L. De Stefano, *Molecules*, 2019, **24**, 2216.
33. R. Chhasatia, M. J. Sweetman, B. Prieto-Simon and N. H. Voelcker, *Sensors and Actuators B: Chemical*, 2018, **273**, 1313-1322.
34. K. Urmann, P. Reich, J.-G. Walter, D. Beckmann, E. Segal and T. Scheper, *Journal of Biotechnology*, 2017, DOI: https://doi.org/10.1016/j.jbiotec.2017.01.005.
35. K. Urmann, S. Arshavsky-Graham, J. G. Walter, T. Scheper and E. Segal, *Analyst*, 2016, **141**, 5432-5440.
36. Ö. Kökpinar, J.-G. Walter, Y. Shoham, F. Stahl and T. Scheper, *Biotechnology and Bioengineering*, 2011, **108**, 2371-2379.
37. S. A. Doyle and M. B. Murphy, *US Patent 0142582 A1*, 2005.
38. G. Zhu, M. Lübbecke, J. Walter, F. Stahl and T. Scheper, *Chemical engineering & technology*, 2011, **34**, 2022-2028.
39. J. G. Walter, O. Kökpinar, K. Friehs, F. Stahl and T. Scheper, *Analytical Chemistry*, 2008, **80**, 7372 - 7378.
40. Y. Sasakura, K. Kanda, T. Yoshimura-Suzuki, T. Matsui, S. Fukuzono, M. H. Han and T. Shimizu, *Analytical Chemistry*, 2004, **76**, 6521-6527.
41. M. Meier, T. R. Patel, E. P. Booy, O. Marushchak, N. Okun, S. Deo, R. Howard, K. McEleney, S. E. Harding, J. Stetefeld and S. A. McKenna, *Journal of Biological Chemistry*, 2013, **288**, 35014-35027.
42. H. Zentgraf, M. Frey, S. Schwinn, C. Tessmer, B. Willemann, Y. Samstag and I. Velhagen, *Nucleic Acids Res*, 1995, **23**, 3347-3348.
43. V. Cortez-Retamozo, M. Lauwereys, G. Hassanzadeh Gh., M. Gobert, K. Conrath, S. Muyldermans, P. De Baetselier and H. Revets, *International Journal of Cancer*, 2002, **98**, 456-462.
44. M. M. Alvarez, F. López-Pacheco, J. M. Aguilar-Yañez, R. Portillo-Lara, G. I. Mendoza-Ochoa, S. García-Echauri, P. Freiden, S. Schultz-Cherry, M. I. Zertuche-Guerra, D. Bulnes-Abundis, J. Salgado-Gallegos, L. Elizondo-Montemayor and M. Hernández-Torre, *PLOS ONE*, 2010, **5**, e10176.
45. K. Els Conrath, M. Lauwereys, L. Wyns and S. Muyldermans, *Journal of Biological Chemistry*, 2001, **276**, 7346-7350.
46. D. Kim and A. E. Herr, *Biomicrofluidics*, 2013, **7**, 041501.
47. G. Gaur, D. S. Koktysh and S. M. Weiss, *Advanced Functional Materials*, 2013, **23**, 3604-3614.
48. S. Hu, Y. Zhao, K. Qin, S. T. Retterer, I. I. Kravchenko and S. M. Weiss, *ACS Photonics*, 2014, **1**, 590-597.
49. N. Massad-Ivanir, T. Friedman, A. Nahor, S. Eichler, L. M. Bonanno, A. Sa'ar and E. Segal, *Soft Matter*, 2012, **8**, 9166-9176.
50. A. W. Drake and S. L. Klakamp, *Journal of Immunological Methods*, 2011, **371**, 165-169.
51. J. A. Goode, J. V. H. Rushworth and P. A. Millner, *Langmuir*, 2015, **31**, 6267-6276.
52. W. Limbut, P. Kanatharana, B. Mattiasson, P. Asawatreratanakul and P. Thavarungkul, *Analytica Chimica Acta*, 2006, **561**, 55-61.
53. C. March, J. J. Manclús, Y. Jiménez, A. Arnau and A. Montoya, *Talanta*, 2009, **78**, 827-833.
54. V. B. Kandimalla, N. S. Neeta, N. G. Karanth, M. S. Thakur, K. R. Roshini, B. E. A. Rani, A. Pasha and N. G. K. Karanth, *Biosensors and Bioelectronics*, 2004, **20**, 903-906.
55. A. B. Mattos, T. A. Freitas, V. L. Silva and R. F. Dutra, *Sensors and Actuators B: Chemical*, 2012, **161**, 439-446.
56. B. I. Kurganov, A. V. Lobanov, I. A. Borisov and A. N. Reshetilov, *Analytica Chimica Acta*, 2001, **427**, 11-19.
57. A. V. Hill, *The Journal of Physiology*, 1910, **40**, i-vii.
58. J. Kim, J. Cho, P. M. Seidler, N. E. Kurland and V. K. Yadavalli, *Langmuir*, 2010, **26**, 2599-2608.
59. E. Tenenbaum, N. Ben-Dov and E. Segal, *Langmuir*, 2015, **31**, 5244-5251.
60. G. Socrates, *Infrared and Raman characteristic group frequencies: tables and charts*, John Wiley & Sons, 2004.
61. K. Urmann, J. Modrejewski, T. Scheper and G. Walter Johanna, *Journal*, 2016, **0**.
62. J. Movilli, A. Rozzi, R. Ricciardi, R. Corradini and J. Huskens, *Bioconjugate Chemistry*, 2018, **29**, 4110-4118.
63. L. A. DeLouise, P. M. Kou and B. L. Miller, *Analytical Chemistry*, 2005, **77**, 3222-3230.
64. A. W. Peterson, R. J. Heaton and R. M. Georgiadis, *Nucleic Acids Research*, 2001, **29**, 5163-5168.
65. J. Rousseaux, R. Rousseaux-Prévost and H. Bazin, *Journal of Immunological Methods*, 1983, **64**, 141-146.
66. B. Strehlitz, N. Nikolaus and R. Stoltenburg, *Sensors (Basel, Switzerland)*, 2008, **8**, 4296-4307.
67. A. Chen and S. Yang, *Biosensors and Bioelectronics*, 2015, **71**, 230-242.
68. S. Arshavsky-Graham, N. Massad-Ivanir, E. Segal and S. Weiss, *Analytical Chemistry*, 2019, **91**, 441-467.
69. G. Rong and S. M. Weiss, *physica status solidi (a)*, 2009, **206**, 1365-1368.
70. T. M. Squires, R. J. Messinger and S. R. Manalis, *Nature Biotechnology*, 2008, **26**, 417.
71. Y. Zhao, G. Gaur, S. T. Retterer, P. E. Laibinis and S. M. Weiss, *Analytical Chemistry*, 2016, **88**, 10940-10948.
72. N. A. E. Hopkins, in *Recognition Receptors in Biosensors*, ed. M. Zourob, Springer, New York Dordrecht Heidelberg London, 2010, ch. 12, pp. 451-529.
73. G. T. Hermanson, *Bioconjugate Techniques* Academic Press, 1st edition edn., 1996.
74. D. Wild, *The Immunoassay Handbook: Theory and Applications of Ligand Binding, ELISA and Related Techniques*, Elsevier Science, 2013.
75. H.-M. Haake, A. Schütz and G. Gauglitz, *Fresenius' Journal of Analytical Chemistry*, 2000, **366**, 576-585.
76. Y. Jung, J. Y. Jeong and B. H. Chung, *Analyst*, 2008, **133**, 697-701.
77. A. K. Trilling, J. Beekwilder and H. Zuilhof, *Analyst*, 2013, **138**, 1619-1627.

View Article Online
DOI: 10.1039/D0AN00178C

78. H. Y. Song, X. Zhou, J. Hobley and X. Su, *Langmuir*, 2012, **28**, 997-1004.
79. G. Gauglitz, *Annual Review of Analytical Chemistry*, 2014, **7**, 297-315.
80. A. Kausaite-Minkstimiene, A. Ramanaviciene, J. Kirlyte and A. Ramanavicius, *Analytical Chemistry*, 2010, **82**, 6401-6408.
81. O. Neumann, D. Zhang, F. Tam, S. Lal, P. Wittung-Stafshede and N. J. Halas, *Analytical Chemistry*, 2009, **81**, 10002-10006.
82. A.-E. Radi and C. K. O'Sullivan, *Chemical Communications*, 2006, DOI: 10.1039/B606804A, 3432-3434.
83. T. Mairal, V. Cengiz Özalp, P. Lozano Sánchez, M. Mir, I. Katakis and C. K. O'Sullivan, *Analytical and Bioanalytical Chemistry*, 2008, **390**, 989-1007.
84. J.-O. Lee, H.-M. So, E.-K. Jeon, H. Chang, K. Won and Y. H. Kim, *Analytical and Bioanalytical Chemistry*, 2008, **390**, 1023-1032.
85. R. C. F. Cheung, J. H. Wong and T. B. Ng, *Applied Microbiology and Biotechnology*, 2012, **96**, 1411-1420.
86. J.-G. Walter, F. Stahl and T. Scheper, *Engineering in Life Sciences*, 2012, **12**, 496-506.
87. G. P. Anderson, M. A. Jacoby, F. S. Ligler and K. D. King, *Biosensors and Bioelectronics*, 1997, **12**, 329-336.

View Article Online
DOI: 10.1039/D0AN00178C

TOC Text:

Aptamers and antibodies are compared as capture probes in a porous silicon-based optical biosensor for detection of a target protein.

View Article Online
DOI: 10.1039/D0AN00178C

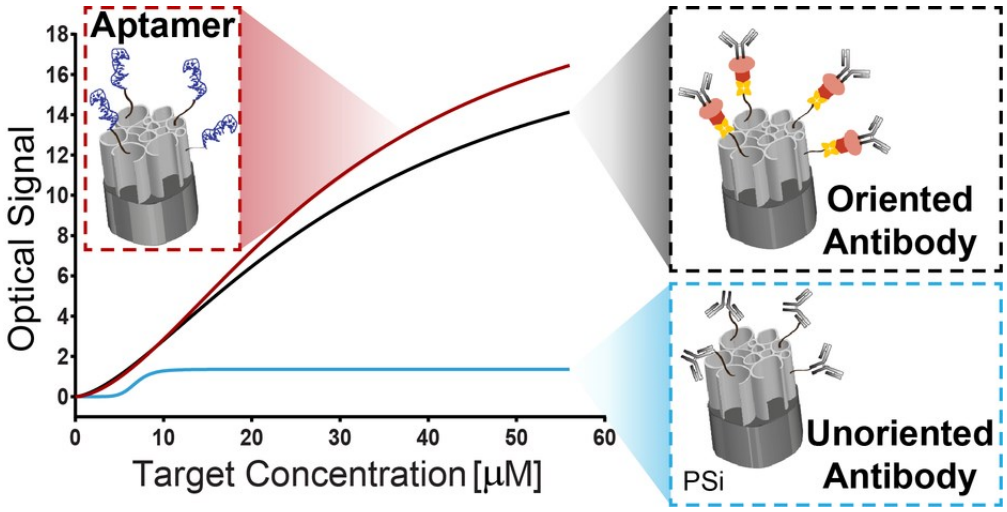

79x39mm (300 x 300 DPI)